Structures of Rat Cytosolic PEPCK: Insight into the Mechanism of Phosphorylation and Decarboxylation of Oxaloacetic Acid[†,‡]

Sarah M. Sullivan and Todd Holyoak*

Department of Biochemistry and Molecular Biology, The University of Kansas Medical Center, Kansas City, Kansas 66160

Received May 28, 2007; Revised Manuscript Received June 21, 2007

ABSTRACT: The structures of the rat cytosolic isoform of phosphoenolpyruvate carboxykinase (PEPCK) reported in the PEPCK-Mn^{2+}, -Mn^{2+}-oxaloacetic acid (OAA), -Mn^{2+}-OAA-Mn^{2+}-guanosine-5′-diphosphate (GDP), and -Mn^{2+}-Mn^{2+}-guanosine-5′-tri-phosphate (GTP) complexes provide insight into the mechanism of phosphoryl transfer and decarboxylation mediated by this enzyme. OAA is observed to bind in a number of different orientations coordinating directly to the active site metal. The Mn^{2+}-OAA and Mn^{2+}-OAA-Mn^{2+}GDP structures illustrate inner-sphere coordination of OAA to the manganese ion through the displacement of two of the three water molecules coordinated to the metal in the holo-enzyme by the C3 and C4 carbonyl oxygens. In the PEPCK-Mn^{2+}-OAA complex, an alternate bound conformation of OAA is present. In this conformation, in addition to the previous interactions, the C1 carboxylate is directly coordinated to the active site Mn^{2+}, displacing all of the waters coordinated to the metal in the holo-enzyme. In the PEPCK-Mn^{2+}-GTP structure, the same water molecule displaced by the C1 carboxylate of OAA is displaced by one of the γ-phosphate oxygens of the triphosphate nucleotide. The structures are consistent with a mechanism of direct in-line phosphoryl transfer, supported by the observed stereochemistry of the reaction. In the catalytically competent binding mode, the C1 carboxylate of OAA is sandwiched between R87 and R405 in an environment that would serve to facilitate decarboxylation. In the reverse reaction, these two arginines would form the CO_2 binding site. Comparison of the Mn^{2+}-OAA-Mn^{2+}GDP and Mn^{2+}-Mn^{2+}GTP structures illustrates a marked difference in the bound conformations of the nucleotide substrates in which the GTP nucleotide is bound in a high-energy state resulting from the eclipsing of all three of the phosphoryl groups along the triphosphate chain. This contrasts a previously determined structure of PEPCK in complex with a triphosphate nucleotide analogue in which the analogue mirrors the conformation of GDP as opposed to GTP. Last, the structures illustrate a correlation between conformational changes in the P-loop, the nucleotide binding site, and the active site lid that are important for catalysis.

The incidence of type 2 (noninsulin-dependent) diabetes mellitus has increased drastically due to the rising prevalence of obesity. This disease is characterized initially by insulin resistance, which is followed by impaired insulin production, resulting in hyperglycemia. Research has concluded that abnormal liver glucose metabolism, including an increase in hepatic glucose production, is due in part to a rise in gluconeogenesis (*1*).

Responsible for the first committed step of gluconeogenesis, phosphoenolpyruvate carboxykinase (PEPCK)[1] is a nucleotide triphosphate (NTP)-dependent enzyme that catalyzes the reversible decarboxylation and concomitant phosphorylation of oxaloacetic acid (OAA) to form phosphoenolpyruvate (PEP) as shown in Scheme 1. PEPCK is a metal-requiring enzyme demonstrating an absolute requirement on divalent cations for activity (*2*−*5*) with Mn^{2+} typically being the most activating cation in the guanosine-5′-triphosphate (GTP)-dependent isoforms. An additional metal ion is required in the form of the nucleotide metal substrate.

Although once widely considered to be the rate-controlling enzyme of gluconeogenesis, recent work has suggested that a number of factors in addition to PEPCK activity are responsible for fluctuations in gluconeogenesis (*6*). Regardless, it has been demonstrated that overexpression of the cytosolic phosphoenolpyruvate carboxykinase (cPEPCK) gene is sufficient to cause insulin resistance and hepatic glucose overproduction (*7*). In addition, RNAi gene silencing of hepatic cPEPCK is sufficient to overcome diabetes-induced hyperglycemia in diabetic mice (*8*). While cPEPCK activity is known to be controlled at the level of gene transcription primarily through the effects of insulin and glucagon (*9*−*12*), recent work has suggested a possible mechanism of regulation for the mitochondrial isozyme

[†] Use of the Advanced Photon Source was supported by the U.S. Department of Energy, Basic Energy Sciences, Office of Science, under Contract no. W-31-109-Eng-38. Use of the BioCARS Sector 14 was supported by the National Institutes of Health, National Center for Research Resources, under Grant no. RR07707.

[‡] Coordinates and structure factors have been deposited in the RCSB protein databank (http://www.rcsb.org/pdb) under the accession codes 2QEW, 2QEY, 2QF1 and 2QF2.

* To whom correspondence should be addressed. Tel: 913-588-0795. Fax: 913-588-7440. E-mail: tholyoak@kumc.edu.

[1] Abbreviations: ASU, asymmetric unit; cPEPCK, cytosolic phosphoenolpyruvate carboxykinase; DTT, dithiothreitol; GDP, guanosine-5′-diphosphate; GTP, guanosine-5′-triphosphate; IPTG, isopropyl-β-D-thiogalactopyranoside; ITP, inosine-5′-triphosphate; ITPγS, inosine-5′-*O*-(3-thio)triphosphate; mPEPCK, mitochondrial phosphoenolpyruvate carboxykinase; NCS, noncrystallographic symmetry; NDP, nucleotide diphosphate; NIDD, noninsulin dependent diabetes; NTP, nucleotide triphosphate; OAA, oxaloacetic acid; PEG, polyethylene glycol; PEP, phosphoenolpyruvate; PEPCK, phosphoenolpyruvate carboxykinase; RMSD, root-mean-square deviation; TLS, translation/libration/screw.

10.1021/bi701038x CCC: $37.00
Published on Web 08/09/2007

Scheme 1: Reversible Decarboxylation and Phosphorylation of OAA Catalyzed by PEPCK

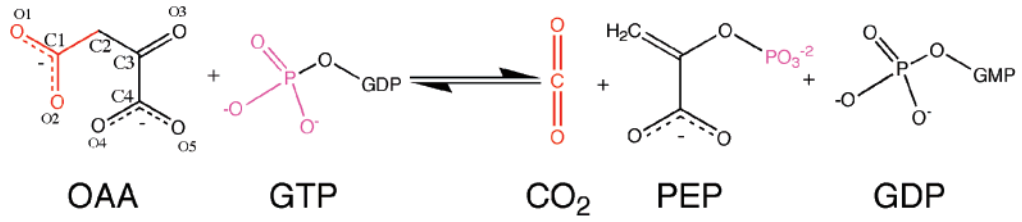

operating at the enzyme level via a transition between an inactive tetrahedral and an active octahedral coordination geometry about the active site manganese ion involving the conserved P-loop cysteine residue (*13*).

Two classes of PEPCKs have been defined based upon their nucleotide specificity: ATP-dependent (EC 4.1.1.49) and GTP (or inosine-5′-triphosphate, ITP)-dependent (EC 4.1.1.32). In addition, the GTP-utilizing enzyme exists as both cytosolic (cPEPCK) and mitochondrial (mPEPCK) isoforms in higher eukaryotes, with the relative ratio of the two enzymes being organism-dependent (*10*). The work presented here is carried out using the cPEPCK isozyme from rat that is an excellent model for the human enzyme as the two enzymes share 92% identity.

While the ATP and GTP isoforms share little sequence identity, the structures of the active sites are reasonably conserved. It has therefore been proposed that an evolutionarily conserved mechanism of catalysis exists between the two classes with phosphoryl transfer occurring through a direct inline transfer of the phosphoryl group progressing through an enol-pyruvate intermediate (*14*−*20*). Mechanistic features have been proposed using data from both the ATP- and the GTP-dependent isozymes (*13*−*16*, *21*−*23*). Inversion of configuration and the orientation of phosphate donor and acceptor strongly support a direct inline mechanism of phosphoryl transfer (*19*, *20*), and the enzyme in complex with AlF_3 has strengthened the argument for an associative transition state (*16*). No consensus has been reached over whether or not decarboxylation and phosphorylation of OAA occur in a stepwise or concerted fashion, as there is evidence for both (*5*, *17*, *24*).

Structures of the human cPEPCK enzyme provided the first glimpse of a GTP-dependent PEPCK and illustrated several differences between the ATP- and the GTP-utilizing enzymes (*21*). As previously suggested, many similarities do exist as most of the proposed active site residues are conserved between the two classes. Further insight into the mechanism of PEPCK catalysis was provided through structural analyses of mitochondrial PEPCK isolated from chicken liver in complex with Mn^{2+}, Mn^{2+}-PEP, and Mn^{2+}-malonate- Mn^{2+}-guanosine-5′-diphosphate (GDP) (*13*). This body of work focused on three features: First, the role of a dynamic loop that becomes ordered in the malonate-nucleotide structure, gating access to the active site and clashing with the observed position of PEP in the PEP-bound complex. Based upon the structural studies, the authors postulated that this loop, designated the "active site lid", was involved in forcing PEP toward inner-sphere coordination to the metal. Second, the tetrahedral coordination of a hyperreactive cysteine to the active site metal in the holo-enzyme suggested a role in enzyme regulation and stimulation of nucleotide product release. Third, a novel conformation of the P-loop suggested a role for S286 in the mechanism of phosphoryl transfer.

The work described here provides further insight into the mechanism of PEPCK catalysis. The structures of rat liver cytosolic PEPCK complexed with Mn^{2+}, Mn^{2+}-OAA, Mn^{2+}-OAA-Mn^{2+}GDP, and Mn^{2+}-Mn^{2+}GTP were determined by X-ray crystallography and demonstrate the direct inner-sphere coordination of OAA to the active site Mn^{2+} and the interactions between the OAA and the enzyme that facilitate decarboxylation. In addition, the complex with the authentic GTP nucleotide demonstrates a dramatic difference in the bound nucleotide conformation from that observed in the GDP and the β,γ-methylene GTP analogue structures (*13*, *21*). This conformation results in the triphosphate group being fully eclipsed in a high-energy state to facilitate phosphoryl transfer.

MATERIALS AND METHODS

Glutathione Uniflow Resin was purchased from Clontech, and HEPES and $MnCl_2$ were obtained from Fisher. Synperonic NP30, polyethylene glycol (PEG) 400, and PEG 3350 were purchased from Fluka. GDP, GTP, OAA, and thrombin were obtained from Sigma. HiQ and P6DG resins were from Bio-Rad. Crystallographic supplies were from Hampton Research. All other materials were of the highest grade available.

Enzyme Expression and Purification. Overnight cultures of BL-21 *Escherichia coli* cells transformed with the plasmid [rat cytosolic PEPCK gene as a C-terminal fusion to glutathione S-transferase in pGEX-4T-2 (GE Biosciences) was provided by Thomas Nowak (University of Notre Dame) and originally cloned by Dr. Yoo-Warren (Bayer Laboratories)] were grown at 37 °C in LB media supplemented with 200 μg/mL ampicillin. The overnight cultures were diluted 40-fold and grown in LB-200 μg/mL ampicillin at 37 °C until the OD_{600} reached 1.0−1.4. The cells were subsequently induced with 1 mM isopropyl-β-D-thiogalactopyranoside (IPTG) and grown for an additional 4 h. Cells were harvested by centrifugation and stored at −80 °C. The frozen pellets were resuspended in buffer A [25 mM HEPES, pH 7.5, 1 mM dithiothreitol (DTT), 10% glycerol, 0.1% Synperonic NP30, 100 mM NaCl, and 0.1 mM EDTA] and lysed by passage through a French pressure cell. Cell debris was pelleted by centrifugation at 8000 rpm for 15 min at 4 °C. The supernatant was incubated with glutathione-Uniflow resin for 1 h at 4 °C, and the resin was washed with buffer A until the A_{280} of the flow-through was less than 0.1. The resin was resuspended in a minimal amount of buffer A and incubated overnight at 4 °C with 20 U of thrombin/mg of predicted fusion protein. The resultant cleaved protein has two additional amino acids (glycine and serine) at the amino terminus. The protein was collected and concentrated by

Amicon to a volume of less than 20 mL. This volume was loaded onto a HiQ column equilibrated in buffer B (25 mM HEPES, pH 7.5, and 1 mM DTT) and washed to remove detergent. PEPCK was eluted by a gradient of NaCl (0−500 mM) and concentrated by Amicon to a volume of less than 2 mL. The collected protein was passed over a P6DG column equilibrated in buffer B with a 1 cm bed of chelex resin on top. The protein was concentrated to final concentration of 10 mg mL^{-1}. The concentration of PEPCK was determined using the extinction coefficient (ϵ_{280}) of 1.60 mL mg^{-1} and a molecular mass of 69560 Da using the ProtParam tool (http://ca.expasy.org/tools/protparam.html) (*25*).

Crystallization. Initial crystallization conditions were determined by submission of PEPCK to the high-throughput crystal screening service at the Hauptman-Woodward Institute (Buffalo, NY; http://www.hwi.buffalo.edu/High_Through/High_Through.html) (*26*). Further optimization of the initial crystallization conditions was performed by hanging-drop vapor diffusion. Crystals of PEPCK used for data collection were grown by the hanging-drop method at 25 °C by mixing 4 μL of protein [containing 10 mg/mL PEPCK, 25 mM HEPES (pH 7.5), and 1 mM DTT] with 2 μL of mother liquor [0.1 M HEPES (pH 7.4) and 12−30% PEG 3350 depending on the complex crystallized] and 0.5 μL of 0.1 M $MnCl_2$. Crystals in complex with Mn^{2+}GDP or Mn^{2+}-GTP were grown by the addition of 0.5 μL of 0.1 M GDP (GTP) in 1 M HEPES, pH 7.4, to the initial drop. Crystals in complex with OAA were obtained by soaking the PEPCK-Mn^{2+} or PEPCK-Mn^{2+}-Mn^{2+}GDP crystals for 1 h in a cryoprotectant solution containing 10 mM OAA prior to crycooling in liquid nitrogen. The PEPCK-Mn^{2+}, PEPCK-Mn^{2+}-OAA, PEPCK-Mn^{2+}-OAA- Mn^{2+}GDP, and PEPCK-Mn^{2+}-Mn^{2+}GTP crystals were cryoprotected by transferring the crystals to 20 μL drops containing 25% PEG 3350, 10% PEG 400, 0.1 M HEPES, pH 7.5, and 2 mM $MnCl_2$, in addition to an equivalent concentration of substrate as the initial drop from which the crystals grew. All crystals were cryocooled prior to data collection by immersion in liquid nitrogen.

Data Collection. Data on the cryocooled crystals of the PEPCK-Mn^{2+} and PEPCK-Mn^{2+}-OAA complexes kept at 100 K were collected using a RU-H3R rotating Cu anode X-ray generator with Blue Confocal Osmic Mirrors and a Rigaku Raxis IV++ detector. Data on the cryocooled crystals of the PEPCK-Mn^{2+}-OAA and PEPCK-Mn^{2+}-OAA-Mn^{2+}GDP crystals maintained at 100k were collected at the Advanced Photon Source, BioCARS 14BMC (Argonne, IL). All data were integrated and scaled with HKL-2000 (*27*). Data statistics are presented in Table 1.

Structure Determination and Refinement. The structure of the rat cytosolic enzyme was determined by molecular replacement using MOLREP (*28*) in the CCP4 (*29*) package and the previously determined structure of human cPEPCK [PDB 1KHG (*21*)]. This molecular replacement solution was refined using Refmac5 followed by manual model adjustment and rebuilding using COOT (*30*). Ligand, metal, and water addition and validation were also performed in COOT.

Inspection of the $F_o - F_c$ maps indicated that in the PEPCK-Mn^{2+}-OAA structure, two conformations of bound OAA were present. The occupancy of the two conformations was manually adjusted (0.5) to minimize positive and negative difference density peaks in the maps and resulted in B-factors for the ligands that were similar to the coordinating residues. In the PEPCK-Mn^{2+}-OAA-Mn^{2+}GDP complex, inspection of the $F_o - F_c$ maps after modeling of the major conformation of GDP in molecule A revealed positive density in the location of the GDP molecule observed in molecule B (Figure 1, Supporting Information). The alternate conformation for the nucleotide was modeled into the density, and its occupancy was adjusted (0.3) following the same criteria as above. The $F_o - F_c$ density also revealed that the P-loop and nucleotide metal were present at a similar occupancy in the same conformation as observed in molecule B, consistent with the alternate conformation of the nucleotide. The alternate conformations for the metal and residues 285−289 of the P-loop were subsequently modeled at the same occupancy as the minor conformation of the nucleotide (0.3). In addition, the occupancy of the closed lid domain (residues 464−474) was manually adjusted to 0.8 resulting in B-factors consistent with the neighboring residues and eliminating the observed negative $F_o - F_c$ difference density. Because PEPCK catalyzes the nucleotide diphosphate (NDP)-dependent decarboxylation of OAA (*31*, *32*), the OAA present in the PEPCK-Mn^{2+}-OAA-Mn^{2+}GDP complex suffers from decarboxylation as was evident by the B-factors for the C1 carboxylate being approximately twice that of the remainder of the OAA molecule. To correct for this, the occupancy of OAA was decreased such that the B-factors for the C1 carboxylate were similar to the rest of the atoms in the molecule. To account for the positive difference density that appeared in the location of the C2-C3-C4 skeleton, pyruvate was added at an occupancy so that the total occupancy of the ligands equals 1.0. This approach resulted in overall B-factors for the ligands that were similar to the coordinating residues and minimized the $F_o - F_c$ difference density. The occupancy and B-factors for the ligands are given in Table 1.

A final round of translation/libration/screw (TLS) refinement was performed for all models in Refmac5. In the PEPCK-Mn^{2+} and PEPCK-Mn^{2+}-OAA structures, a total of 15 TLS groups were utilized while in the PEPCK-Mn^{2+}-OAA-Mn^{2+}GDP and PEPCK-Mn^{2+}-GTP structures a total of 10 TLS groups were utilized per chain. The optimum TLS groups were determined by submission of the pdb files to the TLSMD server (http://skuld.bmsc.washington.edu/~tlsmd/index.html; *33*). In addition, in the PEPCK-Mn^{2+}-OAA-Mn^{2+}-Mn^{2+}GDP complex, tight noncrystallographic symmetry (NCS) restraints were utilized during the initial rounds of refinement and were removed during the final stages of refinement. All of the models have excellent stereochemistry as determined by PROCHECK (*34*). In the PEPCK-Mn^{2+} and PEPCK-Mn^{2+}-Mn^{2+}GTP structures, H6 is found to be a Ramachandran outlier and is modeled as such into well-defined density. Final model statistics are presented in Table 1.

RESULTS

Rat cPEPCK crystallizes as a single molecule in the asymmetric unit (ASU) in the PEPCK-Mn^{2+}, PEPCK-Mn^{2+}-OAA, and PEPCK-Mn^{2+}-Mn^{2+}GTP complexes, whereas two molecules are present in the PEPCK-Mn^{2+}-OAA-Mn^{2+}GDP ASU; these two molecules differ in the state of the active site lid and the conformation of bound OAA and GDP.

Table 1: Data and Model Statistics for the PEPCK -Mn^{2+}, PEPCK -Mn^{2+}-OAA, PEPCK -Mn^{2+}-OAA- Mn^{2+}GDP, and PEPCK -Mn^{2+}-Mn^{2+}GTP Complexes[a]

	PEPCK-Mn^{2+}	PEPCK-Mn^{2+}-OAA	PEPCK-Mn^{2+}-OAA-Mn^{2+}GDP	PEPCK-Mn^{2+}- Mn^{2+} GTP
X-ray source	KUMC-rotating anode	BioCARS 14BMC	BioCARS 14BMC	KUMC-rotating anode
wavelength (Å)	1.54	0.90	0.90	1.54
space group	$P2_1$	$P2_1$	$P2_1$	$P2_1$
unit cell	$a = 44.4$ Å $b = 119.0$ Å $c = 60.6$ Å $\alpha = \gamma = 90.0°$ $\beta = 109.6°$	$a = 45.2$ Å $b = 119.3$ Å $c = 60.8$ Å $\alpha = \gamma = 90°$ $\beta = 108.7°$	$a = 63.5$ Å $b = 119.1$ Å $c = 86.7$ Å $\alpha = \gamma = 90°$ $\beta = 107.4°$	$a = 44.7$ Å $b = 118.9$ Å $c = 60.7$ Å $\alpha = \gamma = 90°$ $\beta = 108.8°$
resolution limit (Å)	24.3−1.8	24.5−1.8	33.3−1.65	32.6−1.90
no. of unique reflections	50729	47649	135193	39968
completeness[b] (%; all data)	97.8 (90.5)	89.3 (43.8)	96.5 (77.9)	89.2 (39.2)
redundancy[b]	7.3 (5.5)	7.0 (5.5)	6.9 (5.9)	6.7 (3.8)
$I/\sigma_{(I)}$[b]	23.4 (2.6)	22.1 (2.6)	22.8 (2.3)	13.8 (1.9)
R_{merge}[b,c]	0.06 (0.46)	0.06 (0.43)	0.06 (0.49)	0.08 (0.50)
no. of ASU molecules	1	1	2	1
solvent content (%)	44.2	43.6	43.5	42.7
R_{free}[b,d] (%)	21.3 (36.1)	22.8 (30.1)	23.8 (32.2)	22.7 (40.9)
R_{work}[b,e] (%)	18.0 (30.1)	19.4 (25.8)	20.5 (28.8)	19.3 (33.8)
average B values[f]				
protein	19.4	29.8	17.6	19.3
water	32.8	40.8	35.6	31.2
OAA	NA	$OAA_1 = 32.4$, oc = 0.5 $OAA_2 = 30.9$, oc = 0.5	Mol A: 24.3, oc = 0.4 Mol B: 26.3, oc = 0.4	NA
pyruvate	NA	NA	Mol A: 17.4, oc = 0.6 Mol B: 27.0, oc = 0.6	NA
GDP	NA	NA	Mol A: $GDP_1 = 20.3$, oc = 0.7 GDP_2, 18.5 oc = 0.3 Mol B: 27.7, oc =1.0	NA
GTP	NA	NA	NA	21.4
estimated coordinate error based on maximum likelihood (Å)	0.08	0.11	0.09	0.12
bond length RMSD (Å)	0.008	0.008	0.009	0.006
bond angle RMSD (deg)	1.08	1.12	1.19	1.00
Ramachandran statistics (most favored, additionally allowed, generously allowed, disallowed) (%)	90.3, 8.9, 0.6, 0.2	90.7, 8.9, 0.4, 0.0	90.9, 8.5, 0.4, 0.2	90.8, 8.6, 0.4, 0.2

[a] NA, not applicable; Mol A, molecule A of the crystallographic dimer; Mol B, molecule B of the crystallographic dimer; oc, ligand occupancy. OAA_1 and OAA_2 correspond to the two alternate conformations of OAA illustrated in Figure 2. GDP_1 and GDP_2 are the two conformations of GDP present in the A molecule of the PEPCK-Mn^{2+}-OAA-Mn^{2+}GDP crystallographic dimer. [b] Values in parentheses represent statistics for data in the highest resolution shells. The highest resolution shell comprises data in the range of 1.86−1.80, 1.86−1.80, 1.71−1.65, and 1.97−1.90 Å for the PEPCK-Mn^{2+}, PEPCK-Mn^{2+}-OAA, PEPCK-Mn^{2+}-OAA-Mn^{2+}GDP, and PEPCK-Mn^{2+}-Mn^{2+}GTP data sets, respectively. [c] $R_{merge} = \Sigma|I_{obs} - I_{avg}|/\Sigma I_{obs}$. [d] See Brunger (*45*) for a description of R_{free}. [e] $R_{work} = \Sigma||F_{obs}| - |F_{calcd}||/\Sigma|F_{obs}|$. [f] B values indicated are residual B values after TLS refinement.

All models are complete with the exception of the active site lid, comprised of amino acids 464−473, for which there is no density except in molecule A of the PEPCK-Mn^{2+}-OAA- Mn^{2+}GDP complex. PEPCK is expressed as a C-terminal fusion to glutathione-S-transferase. Cleavage of the expressed protein with thrombin leads to the presence of an additional glycine and serine residue preceding the N-terminal methionine of PEPCK. These residues, in addition to the first two native residues of PEPCK in the PEPCK-Mn^{2+} and PEPCK-Mn^{2+}-Mn^{2+}GTP complexes and the first nine native residues in the PEPCK-Mn^{2+}-OAA and PEPCK-Mn^{2+}-OAA-Mn^{2+}GDP complexes, are not included in the models. Data and model statistics for all models are presented in Table 1.

PEPCK-Mn^{2+}. In accordance with the high degree of sequence identity between the rat cPEPCK and the avian mitochondrial (64%) and human cytosolic (92%) isoforms, superpositioning of the holo-enzyme with the previously solved structures confirmed a virtually identical overall fold, with an overall C_α root-mean-square deviation (RMSD) of 0.94 and 0.76 Å, respectively.

As determined by previous NMR and crystallographic studies of the human and chicken mitochondrial isoforms, the active site manganese ion is seen in octahedral geometry, coordinated to K244, H264, D311, and three water molecules (Figure 1) (*5*, *13*, *21*, *35*, *36*). Contrary to what was observed in the mPEPCK holo-enzyme, no evidence for a tetrahedral geometry about the active site manganese ion, involving the reactive cysteine (C288), is seen. Like the human cPEPCK enzyme, this is most likely due to the presence of reducing agent (1 mM DTT) in the crystallization conditions.

PEPCK-Mn^{2+}-OAA. Prior to this work, information on the interaction of OAA with PEPCKs came from the ATP-utilizing PEPCKs from *E. coli* (*16*, *37*) and *Anaerobiospirillum succiniciproducens* (*38*) using oxalate and pyruvate as analogues of OAA. The structure of the PEPCK-Mn^{2+}-OAA complex demonstrates, for the first time, inner-sphere coordination of OAA to the active site metal and illustrates two different modes of OAA binding (Figures 2 and 3A,B). The first conformation (OAA_1), also seen in the PEPCK-Mn^{2+}-OAA-Mn^{2+}GDP complex (Figure 4), shows O3 and O5 directly coordinated to the active site manganese (Figure

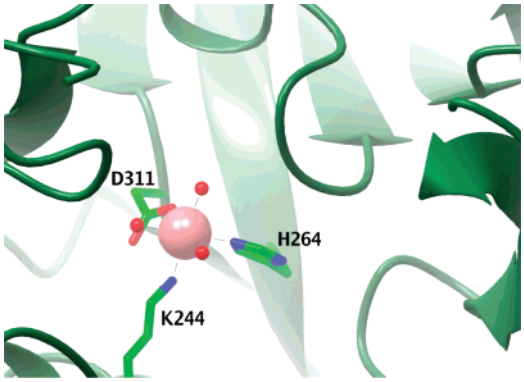

FIGURE 1: Active site structure of the holo-enzyme form of rat cPEPCK. The active site manganese ion (pink sphere) is coordinated in octahedral geometry by the side chains of K244, H264, D311, and three water molecules (shown as red spheres). The dashed lines indicate metal−ligand interactions. All figures were generated using CCP4MG (*46*, *47*).

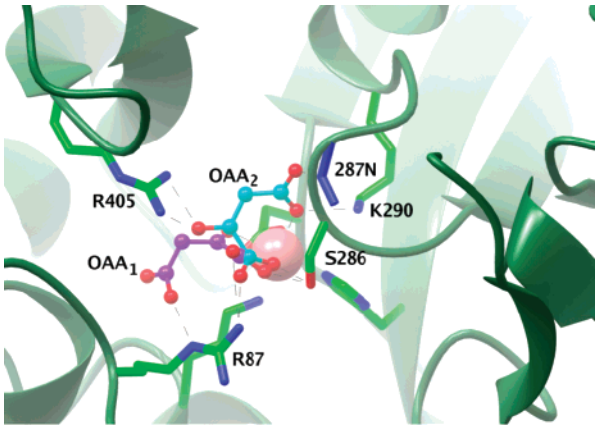

FIGURE 2: Active site structure of the PEPCK-Mn^{2+}-OAA complex. Shown are the two conformations of OAA in direct inner-sphere coordination to the active site manganese ion; the catalytically competent form (OAA_1, purple) is also seen when PEPCK is bound to OAA and GDP. In the second, catalytically inactive conformation (OAA_2, light blue), the C1 carboxylate is coordinated to the active site manganese ion resulting in the nucleophilic C3 carbonyl turning away from the metal. The dashed lines indicate potential hydrogen bonds and metal−ligand interactions.

3B). O5 also interacts with the P-loop S286, while O4 interacts with the NH2 of R87 and NH1 of R405. The C1 carboxylate is extended away from the metal and sandwiched between the side chains of R87 and R405, leading to an interaction between the O2 and the Nϵ of R87 (Figure 3B). In the second bound conformation (OAA_2), the C1 carboxylate has flipped toward the active site manganese, allowing direct coordination of O2 to the metal and interacting with the P-loop through a backbone nitrogen (A287) and K290 (Figures 2 and 3A). O4 maintains its interactions with R87, but the C3 carbonyl is oriented away from metal and instead interacts with R405, rendering this a catalytically incompetent mode of binding (Figure 3A).

PEPCK-Mn^{2+}-OAA-Mn^{2+}GDP. The structure of the PEPCK-Mn^{2+}-OAA-Mn^{2+}GDP complex results in two molecules being present in the ASU; in molecule A, the active site lid (residues 464−473) is closed, whereas in molecule B, and all other models reported here, the lid is disordered and not modeled (Figure 4). In addition, the occupancy of the C1 carboxylate of OAA is reduced as compared to that of the C2-C3-C4 carbon skeleton due to decarboxylation of OAA to form pyruvate and therefore is modeled as a mixture of OAA and pyruvate (Table 1). In both molecules A and B, OAA is found in conformations similar to the catalytically competent form of OAA in the PEPCK-Mn^{2+}-OAA structure, with O3 and O5 coordinated to the active site metal (Figure 3C,D). In molecule B, the bound OAA is identical to that seen in the PEPCK-Mn^{2+}-OAA complex (Figure 3C). In this conformation, the C1 carboxylate interacts directly with the Nϵ of R87. In molecule A (Figure 3D), the C1 carboxylate has shifted slightly, lengthening the interaction with the Nϵ of R87. This interaction is replaced by an interaction between the Nϵ of R87 and O4 (Figure 3D). In both conformations, O4 makes additional contacts with the NH2 of R87 and the NH1 of R405 (Figure 3C,D).

The conformation of GDP in both molecules in the ASU (Figure 4A) is identical to the bound conformation of GDP in the previous malonate-GDP complex with mPEPCK [PDB 2FAH (*13*)] and the β-γ-methylene-GTP analogue in the previously determined human cPEPCK structure [PDB 1KHB (*21*)]. The nucleotide in molecule A differs slightly in its position in the active site pocket relative to the nucleotide in molecule B, with the GDP bound in molecule A being shifted ~1 Å in a direction toward the active site Mn^{2+} (Figure 4). Evidence for the standard GDP conformation found in molecule B being present in molecule A was observed in the $F_o - F_c$ difference density resulting in modeling of the conformation at low occupancy (0.3; Figure 1, Supporting Information). Consistent with the low occupancy of the molecule B nucleotide conformation is the presence of the P-loop and nucleotide metal conformations that are observed in molecule B being present in molecule A in conjunction with the shift in the nucloetide (data not shown). These were modeled at the same occupancy as the minor nucleotide conformation (Table 1, GDP_2). Last, the closed lid domain was modeled at a similar reduced occupancy to minimize the negative difference density and is consistent with the steric conflict that arises between the P-loop position in molecule B and the closed conformation of the lid. The bound conformation of the α- and β-phosphate oxygens in both molecules is staggered with respect to each other, and extensive hydrogen bonding occurs between the phosphate oxygens and the backbone nitrogens of the P-loop, as is consistent with other kinases. The ribose sugar is oriented through interactions with backbone carbonyls and R436; the ring oxygen (O4′) interacts with R436, while the exocyclic oxygens (O2′ and O3′) interact with the backbone carbonyl oxygens of residues P337 (molecule A only) and G338 (molecules A and B) (Figure 5A). The backbone nitrogen of F530 interacts with O6 of the guanidinium ring in addition to an interaction (~3.0 Å) between the ND2 of N533 and the O6 carbonyl that has previously been proposed to act as a selectivity filter between guanosine and adenosine nucleotides (*39*) (Figure 4).

PEPCK-Mn^{2+}- Mn^{2+}GTP. GTP binds to the enzyme in a similar fashion to the GDP found in molecule B of the PEPCK-Mn^{2+}-OAA-Mn^{2+}GDP structure; however, the γ-phosphate oxygens displace one water molecule from the coordination sphere of both the nucleotide and the active site metal ions, thereby acting as a bridging ligand between the two metal centers (Figure 6). There are two distinct structural differences between bound GTP and bound GDP; first, the ribose ring has flipped such that the exocyclic

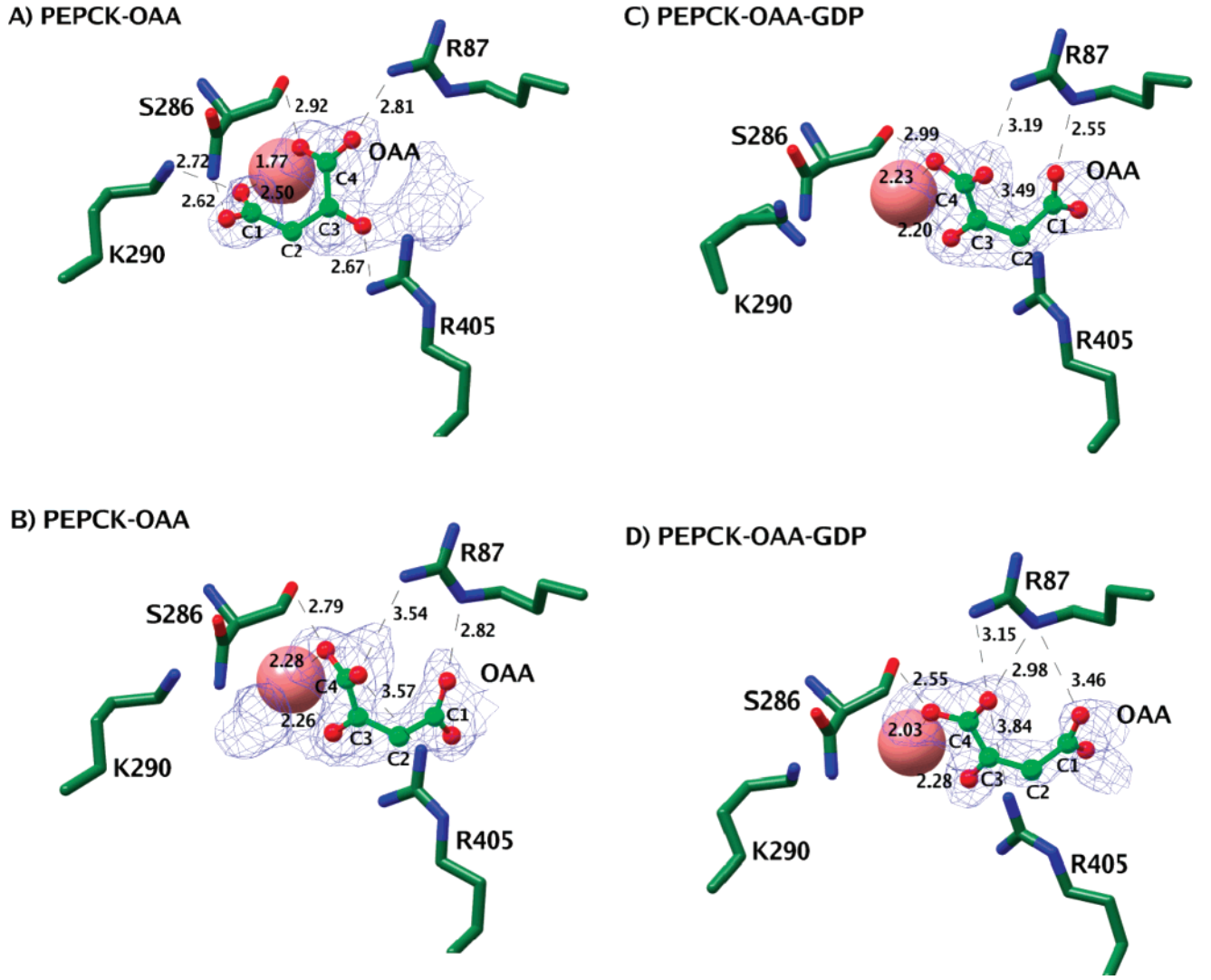

FIGURE 3: Multiple binding modes of OAA in the PEPCK-Mn^{2+}-OAA and PEPCK-Mn^{2+}-OAA-Mn^{2+}GDP complexes. (A) The catalytically incompetent mode of OAA (green ball-and-stick model) binding results from the direct coordination of the C1 carboxylate to the active site manganese ion and a rotation of the nucleophilic C3 carbonyl away from the metal ion. (B−D) The phosphorylation competent forms of OAA with the C1 carboxylate sandwiched between R87 and R405. The C3 carbonyl is perfectly oriented for nucleophilic attack on the γ-phosphate of GTP, and S286 is in intimate contact with the C4 carbonyl. The conformation shown in panel C found in molecule B of the PEPCK-Mn^{2+}-OAA-Mn^{2+}GDP complex is nearly identical to the conformation shown in panel B from the PEPCK-Mn^{2+}-OAA complex. (D) The OAA present in molecule A of the PEPCK-Mn^{2+}-OAA-Mn^{2+}GDP complex is similar to that found in panels B and C; however, minor changes in the position of the C1 carboxylate result in longer interactions between the bound ligand and R87 and R405. The active site metal ligands have been omitted, and the atom numbers for OAA are given for clarity. The dashed lines indicate potential hydrogen bonds, and the distances are indicated in angstroms. The F_o-F_c density rendered at 2.4 σ prior to the inclusion of the ligands into the model is shown as a blue mesh.

oxygen O3′ now interacts with R436 (Figures 5B and 6). This results in a loss of the other interactions between the enzyme and the ribose ring in the GDP complex, described above. In concert, the α-phosphate moves (2.13 Å) from its position in GDP (Figure 7). This movement is accompanied by a rotation of the phosphodiester backbone that results in near eclipsing of the oxygens of the α-phosphate with both the β- and the γ-phosphates, in addition to the well-characterized eclipsing of the terminal β- and γ-phosphate oxygens. This unique conformation results in an even higher energy state for the bound nucleotide than that occurring in typical kinases with only the β- and γ-phosphates being eclipsed (Figure 8). The eclipsed nature of the β- and γ-phosphates is accomplished through stabilization of the β-phosphate by interactions with the backbone nitrogens of the P-loop and the β-phosphate, and the formation of a salt bridge between the R405 and the γ-phosphate (Figure 5B). Additional stabilization of this conformation comes from the interaction of the γ-phosphate with the P-loop lysine K290.

DISCUSSION

Previous structural studies on PEPCK have either focused upon the interaction of PEP with the enzyme (*13*, *21*) or have utilized the competitive inhibitor oxalate or malonate as analogues of a putative enolate intermediate to postulate a mechanism for the phosphorylation of OAA (*13*, *37*, *38*). The work presented here demonstrates the interaction of the authentic OAA and GTP substrates with a GTP utilizing PEPCK and demonstrates that while the conclusions reached with the analogue structures are generally correct, some differences exist, and this new data provides important insight into the mechanism of PEPCK-mediated catalysis.

While two conformations of OAA are present in the PEPCK-OAA complex, only one is positioned such that it

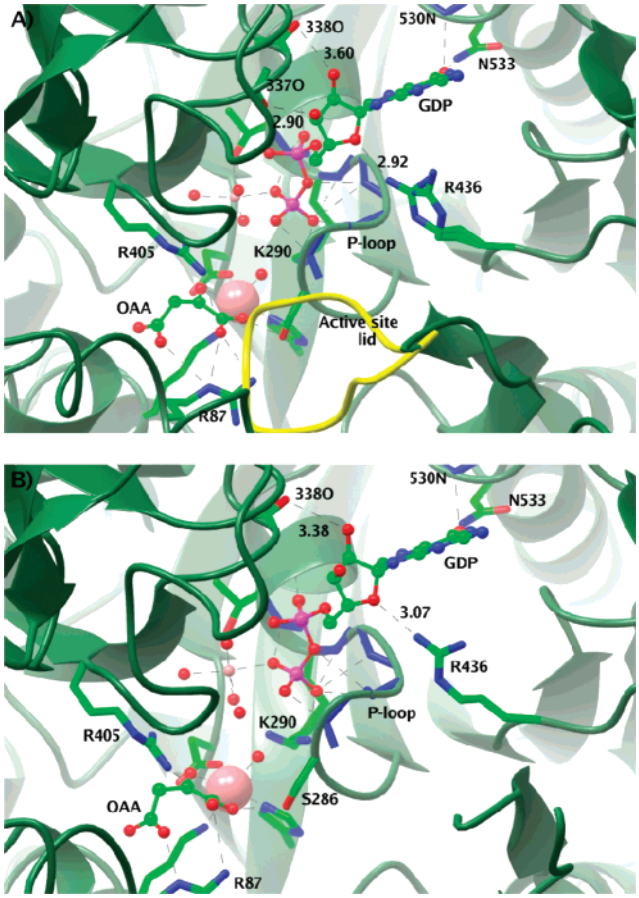

FIGURE 4: Active site structure of the PEPCK-Mn^{2+}-OAA-Mn^{2+}-GDP complex. Both the A (A) and B (B) molecules found in the ASU are shown. These molecules differ in the state of the active site lid (yellow strand) being closed in A and disordered in B and the movement of the nucleotide in molecule A toward the active site manganese ion relative to the position of the nucleotide in molecule B. For simplicity, only the major conformation of GDP present in molecule A is illustrated. The minor conformation is identical to that shown in panel B. Manganese ions are modeled as pink spheres, the larger being the active site manganese. The water molecules coordinating to the active site and nucleotide metals are shown as red spheres. The dashed lines indicate potential hydrogen bonds and metal−ligand interactions. The distances between the atoms interacting with the ribose and base of the nucleotide are indicated in angstroms.

would be catalytically competent (Figures 2 and 3B−D, OAA_1). In the catalytically competent conformation, the O3 and O5 carbonyl oxygens displace two of the three water molecules coordinated to the active site manganese ion in the holo-enzyme and the C1 carboxylate is oriented away from the metal, positioned between R87 and R405. The nucleophilic C3 carbonyl is positioned adjacent to the site on the metal where the O2γ oxygen of the γ-phosphate of GTP coordinates in the enzyme-GTP complex. Superpositioning of the OAA and GTP structures generates a model that shows a collinear relationship between the O3 and the γ-phosphate at a distance of 3.35 Å (Figure 9). This is consistent with previous kinetic studies of cytosolic and mitochondrial PEPCK isozymes that suggest a direct inline mechanism of phosphoryl transfer (*19*, *20*). The sandwiching of the C1 carboxylate between R87 and R405 that is observed in the structures may facilitate decarboxylation through unfavorable interactions with the lone pair electrons of Nϵ of the R87 side chain (Figure 3). In the reverse reaction, the carboxylation of PEP, binding of the linear CO_2 molecule in a similar location to the C1 carboxylate, would allow CO_2 to bridge between the Nϵ of R87 and the NH2 amine of R405, forming the CO_2 binding site. This is consistent with the observation in the chicken mitochondrial enzyme that CO_2 protects the enzyme from inactivation by the chemical modification of arginine residues (*40*). The second conformation of OAA bound in the PEPCK-Mn^{2+}-OAA complex was not expected based upon the previous structures of PEPCK in complex with oxalate (*37*, *38*) (Figure 3A). As mentioned above, in the conformation OAA_1 (Figure 2), O3 and O5 of OAA displace two of the three coordinating water molecules found in holo-enzyme (Figure 1). This leaves a single water molecule remaining in the metal's coordination shell. As this site binds the γ-phosphate of GTP (Figures 5B and 6) and appears to have an affinity for sulfate ions (Sullivan and Holyoak, unpublished data), the observation that the C1 carboxylate of OAA coordinates to this site by displacing the remaining water molecule is consistent with this environment favoring coordination by anions (OAA_2, Figures 2 and 3A). As this orientation also turns the nucleophilic C3 carbonyl away from the metal, it is apparent that this conformation of OAA is not catalytically competent. This conformation (OAA_2) only exists in the absence of nucleotide. As such, this conformation provides a structural rationale for NDP-dependent decarboxylation of OAA catalyzed by the GTP-dependent PEPCKs (*31*, *32*). This nucleotide-dependent decarboxylase activity in the GTP utilizing PEPCKs is in contrast to the decarboxylase activity of the ATP utilizing enzymes from *A. succiniciproducens* and *Saccharomyces cerevisiae*, which do not require the presence of nucleotide to catalyze this activity (*41*). Therefore, the structural data suggest a mechanism whereby upon nucleotide binding the C1 carboxylate is oriented away from the metal toward R87 and R405, repositioning the nucleophilic C3 carbonyl in the correct geometry for nucleophilic attack of the γ-phosphate (Figure 9) or in the presence of the NDP, the enzyme catalyzes the decarboxylation step only, resulting in the formation of pyruvate. This is confirmed by the mixture of OAA and pyruvate found in the PEPCK-Mn^{2+}-OAA-Mn^{2+}GDP complex that is not observed in the PEPCK-Mn^{2+}-OAA complex.

As was seen previously in the structures of mPEPCK (*13*), the aberrant P-loop motif in GTP-PEPCKs is a highly mobile element, and the interactions between the inner-sphere coordinated malonate, OAA, and GTP ligands and S286 suggest an importance of this residue in catalysis. The current structures provide further insight into the role that S286 plays in catalysis. In the complexes with OAA, the S286 hydroxyl group is observed to interact with the C4 carbonyl oxygen (O5) that is cis to the site of phosphorylation, further stabilizing the inner-sphere coordinated OAA molecule (Figure 3). The S286-OAA interaction is the result of the P-loop adopting a fully closed conformation when compared to the position of the loop in the holo-enzyme, molecule B of the GDP complex or the GTP complex. Because this closed conformation is the only conformation present when the active site lid is ordered in a closed orientation, it raises an interesting question of whether the conformational state of the P-loop and the active site lid are coupled. Evidence for this conclusion comes from the analysis of the other complexes. In contrast to the closed conformation of the

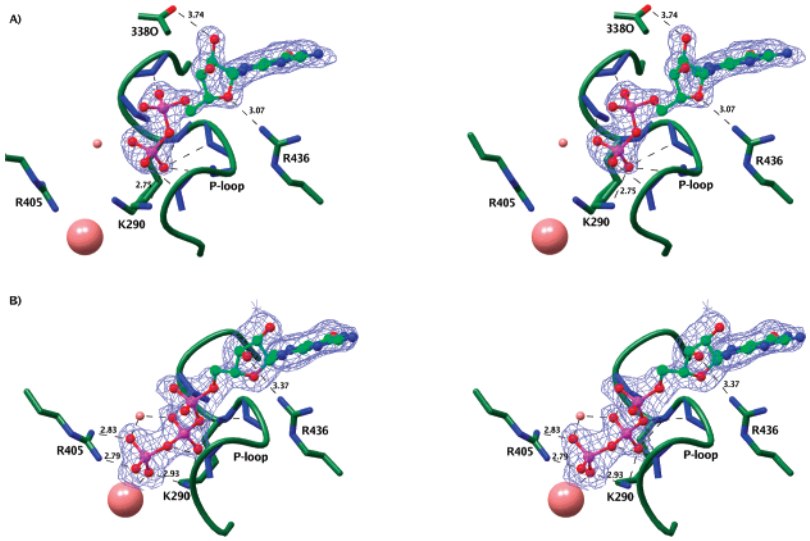

FIGURE 5: Stereoview representation comparing the interactions between PEPCK and (A) GDP and (B) GTP nucleotides. The F_o-F_c density rendered at 2.4 σ prior to the inclusion of the ligands into the model is shown as a blue mesh. The interactions differing between the diphosphate and the triphosphate nucleotides are indicated, and the distances are shown in angstroms. Potential hydrogen bonds between the backbone amides of the P loop and the β-phosphate of the nucleotides are indicated with dashed lines. The active site Mn^{2+} is rendered as a large pink sphere while the nucleotide associate Mn^{2+} is shown as a small pink sphere. The water molecules coordinating to the metal ions and the active site metal ligands have been omitted for clarity.

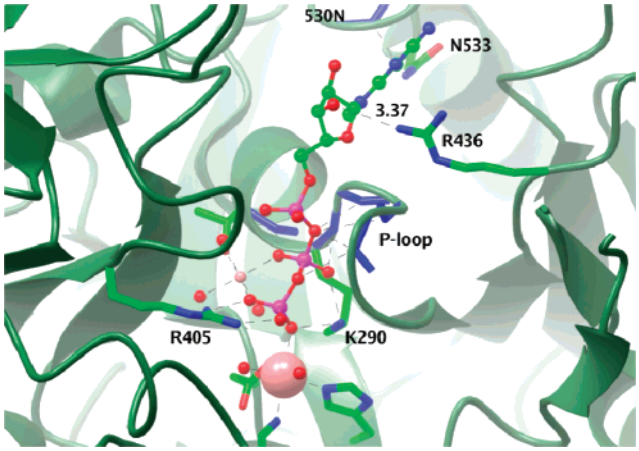

FIGURE 6: Active site structure of the PEPCK-Mn^{2+}-Mn^{2+}GTP complex. Manganese ions are modeled as pink spheres, the larger being the active site manganese. The water molecules coordinating to the active site and nucleotide metals are shown as red spheres. The dashed lines indicate potential hydrogen bonds and metal−ligand interactions. The distance between R436 and O3′ of the ribose ring is indicated in angstroms.

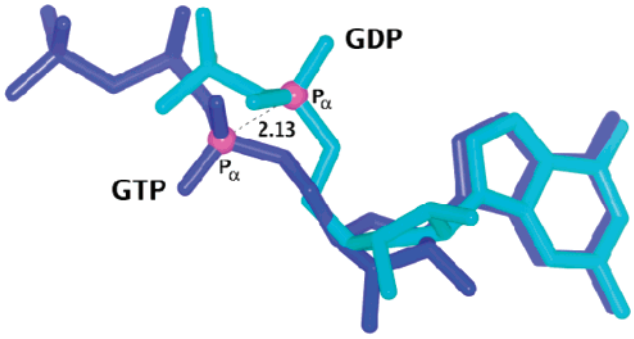

FIGURE 7: Changes in the bound conformation of GDP and GTP. Superpositioning of the PEPCK-Mn^{2+}-OAA-Mn^{2+}GDP and PEPCK-Mn^{2+}-Mn^{2+}GTP structures illustrates the changes in the bound conformation of the ribose and α-phosphate between bound GDP (light blue) and GTP (dark blue). The displacement in the position of the α-phosphate (purple) is shown in angstroms.

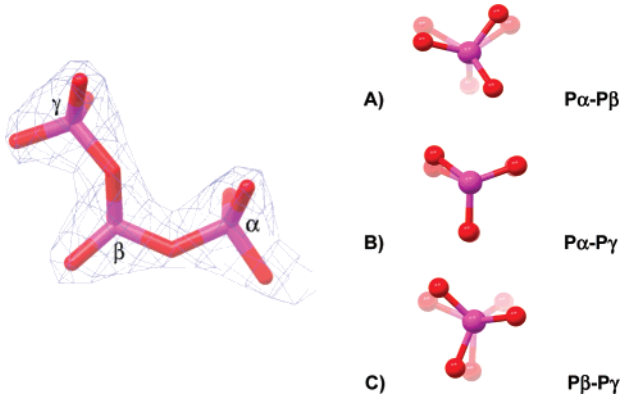

FIGURE 8: Configuration of the GTP phosphate chain in the PEPCK-Mn^{2+}-Mn^{2+}GTP complex. The $2F_o-F_c$ density rendered at 2.5σ for the phosphate chain is shown as a blue mesh. The eclipsed nature of the (A) α-β, (B) α-γ, and (C) β-γ phosphoryl groups is illustrated.

P-loop in molecule A of the OAA-GDP complex, in the B molecule of that same complex and the GTP complex, the P-loop has opened slightly.[2] In the B molecule of the OAA-GDP complex, the slightly opened P-loop repositions the backbone nitrogen of A287, which forms contacts with the β-phosphate of the bound nucleotide, and this conformational change is correlated with a displacement of the bound GDP ~1 Å away from the active site metal when compared with the nucleotide position found in molecule A. In the GTP structure, the more open conformation of the P-loop is stabilized by the interaction of the S286 hydroxyl with the O3γ (3.53 Å) of the inner-sphere coordinated γ-phosphate. Furthermore, the P-loop in the holo-enzyme structure is in a fully open state. In all three of these complexes, the active site lid is open, suggesting a correlation between the position of the P-loop and the active site lid. Inspection of the

[2] The identical conformation of the P loop to that seen in molecule B is also observed in molecule A in conjunction with the minor conformation of the nucleotide (GDP_2).

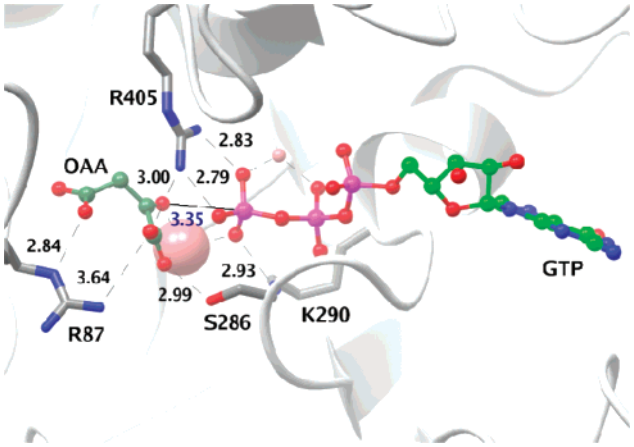

FIGURE 9: Superpositioning of the PEPCK-Mn^{2+}-OAA and PEPCK-Mn^{2+}-Mn^{2+}GTP complexes generates a theoretical Michaelis complex. This complex demonstrates the collinear relationship between the γ-phosphate of GTP and the O3 of OAA. The distance for phosphoryl transfer is shown in angstroms (blue text) and indicated as a solid line. The other important interactions are shown as dashed lines, and the distances are indicated in angstroms. The active site metal ligands have been omitted for clarity. Manganese ions are modeled as pink spheres, the larger being the active site manganese.

structures reveals that the active site lid can only adopt the closed conformation in the presence of the fully closed P-loop, as the other two conformations of the loop result in steric conflict between the Cγ2 of T465 on the lid and the backbone carbonyl of S286 on the P-loop. In the fully closed P-loop conformation, a hydrogen bond between the backbone carbonyl of S286 and the lid T465 side chain hydroxyl group (3.03 Å) in addition to a hydrogen bond between E89 and H470 seems to stabilize the closed lid conformation. Finally, the PEPCK-Mn^{2+}-OAA complex suggests that P-loop closure alone is not sufficient to dictate that the equilibrium position of the active site lid shifts toward a closed state. In the OAA complex, the P-loop adopts a similar closed conformation to that found in molecule A of the PEPCK-Mn^{2+}-OAA-Mn^{2+}GDP complex with the serine hydroxyl interacting with the C4 carbonyl oxygen (O5); however, in the absence of bound nucleotide, the active site lid remains open. Again, comparison of molecule A and B in of the PEPCK-Mn^{2+}-OAA-Mn^{2+}GDP complex provides some insight into how this communication between the P-loop, active site lid, and nucleotide-binding site may occur. In the intermediate and open states of the P-loop, the backbone carbonyl of A287 sterically conflicts with the forward orientation of the R436 side chain seen in molecule A of the PEPCK-Mn^{2+}-OAA-Mn^{2+}GDP complex, whose interaction with the nucleotide ribose coincides with the 1 Å forward shift of the nucleotide seen relative to molecule B and the GTP structure. While it is clear that the state of the two mobile structural elements, namely, the P-loop and the active site lid, and the state of the bound nucleotide are coupled, based on the current experimental evidence it is not possible to determine cause and effect. These results do suggest that in addition to the interactions S286 makes with the C4 carbonyl, facilitating catalysis, S286 may play a role as an allosteric sensor to dictate lid closure through P-loop positioning. We believe that the open nature of the active site pocket and the observation that active site lid closure occurs only upon occupancy of the active site by both OAA and nucleotide are more consistent with a random mechanism of substrate addition than an ordered one, although there is kinetic evidence for both random (*42*) and ordered Bi-Ter mechanisms for rat cPEPCK (*18*).

Previously, the structure of the human cPEPCK isozyme was solved in complex with the β-γ-methylene-GTP analogue, demonstrating the interaction of the γ-phosphate as a bridging ligand between the active site and the nucleotide metals (*21*). This conformation, in addition to the interactions with R405 and the P-loop lysine K290, and the observation that these interactions induce an eclipsed conformation between the β- and the γ-phosphates, was suggested as the mechanism allowing for efficient phosphoryl transfer (*21*) and is consistent with previous kinetic data (*39*, *43*, *44*). While no information on the nature of the transition state for phosphoryl transfer is available on the GTP-utilizing class of PEPCKs, complexes of the *E. coli* ATP-dependent enzyme with AlF_3 are consistent with an associative S_N2-like transition state (*16*). Surprisingly, the structure of the enzyme in complex with the authentic GTP nucleotide demonstrates some interesting differences between the bound conformation of either the GDP or the β-γ-methylene-GTP analogue that are essentially identical to each other (Figure 7). Similar to the GTP analogue complex, the nucleotide base and the β-γ-phosphates of GTP are held in an eclipsed conformation by a salt bridge between the R405 and the γ-phosphate oxygens and several interactions between the P-loop backbone amide nitrogens and the β-phosphate (Figures 4−6). In contrast to the β-γ-methylene-GTP and GDP structures, the position of the α-phosphate and the ribose ring are dramatically different (Figure 7). The complex between GTP and PEPCK results in the enzyme stabilizing a highly unusual fully eclipsed conformation of the phosphodiester backbone, such that the movement of the α-phosphate results in all of the phosphoryl groups being eclipsed with one another (Figure 8). The movement of the α-phosphate occurs in concert with a change in the conformation of the ribose ring, such that this conformation is now stabilized by an interaction between the exocyclic O3′ of the ribose and the NH1 of R436. This new interaction results in the loss of the previous interaction in the GDP and β-γ-methylene-GTP complexes between R436 and O4 of the ribose ring and the interactions of the exocylic oxygens with the peptide backbone between P337 and G338 (Figure 5). This interesting and presumably higher energy state for the authentic GTP molecule may explain the ability of PEPCK to catalyze the transfer of the thiophosphoryl group of inosine-5′-*O*-(3-thio)triphosphate (ITPγS) with similar catalytic efficiency to that of ITP through the further ground state destabilization of the bound nucleotide (*19*, *20*).

Taken together, the structures of rat cytosolic PEPCK presented here provide new insight into the mechanism by which GTP, and perhaps ATP utilizing PEPCKs, catalyze the efficient transfer of the γ-phosphate of GTP to OAA in this important metabolic reaction. The structural data presented are consistent with a mechanism of direct inline phosphoryl transfer. PEPCK also appears to be unique among kinases by stabilizing a potentially higher energy state for the phosphate chain that is typically not seen. Furthermore, the results provide a structural rationale for the observed diphosphate nucleotide dependency of the decarboxylase activity that is unique to the GTP-dependent class of

PEPCKs. Finally, the results illustrate the importance of two dynamic elements in PEPCK catalysis. The results demonstrate a correlation between the state of the mobile P-loop mediated by contacts between OAA and S286, the occupancy of the nucleotide-binding site, and the state of the active site lid. In general, it is hoped that the information gained from all of the structural work will provide the ability to design new and effective inhibitors of PEPCK catalysis as potential noninsulin-dependent diabetes (NIDD) therapies.

NOTE ADDED IN PROOF

While the manuscript was under review, Cotelesage et al. published the structure of *E. coli PEPCK* in complex with ATP and CO_2, demonstrating the interaction of the bound CO_2 molecule with the residues equivalent to R87 and K244 in rat cPEPCK (*48*).

SUPPORTING INFORMATION AVAILABLE

Figure of the two conformations of GDP present in molecule A of the PEPCK-Mn^{2+}-OAA-Mn^{2+}GDP crystallographic dimer. This material is available free of charge via the Internet at http://pubs.acs.org.

REFERENCES

1. Radziuk, J., and Pye, S. (2001) Hepatic glucose uptake, gluconeogenesis and the regulation of glycogen synthesis, *Diabetes Metab. Res. Rev. 17*, 250−272.
2. Lee, M. H., Hebda, C. A., and Nowak, T. (1981) The role of cations in avian liver phosphoenolpyruvate carboxykinase catalysis. Activation and regulation, *J. Biol. Chem. 256*, 12793−12801.
3. Colombo, G., Carlson, G. M., and Lardy, H. A. (1981) Phosphoenolpyruvate carboxykinase (guanosine 5′-triphosphate) from rat liver cytosol. Dual-cation requirement for the carboxylation reaction, *Biochemistry 20*, 2749−2757.
4. Hebda, C. A., and Nowak, T. (1982) The purification, characterization, and activation of phosphoenolpyruvate carboxykinase from chicken liver mitochondria, *J. Biol. Chem. 257*, 5503−5514.
5. Hebda, C. A., and Nowak, T. (1982) Phosphoenolpyruvate carboxykinase. Mn2+ and Mn2+ substrate complexes, *J. Biol. Chem. 257*, 5515−5522.
6. Burgess, S. C., He, T., Yan, Z., Lindner, J., Sherry, A. D., Malloy, C. R., Browning, J. D., and Magnuson, M. A. (2007) Cytosolic phosphoenolpyruvate carboxykinase does not solely control the rate of hepatic gluconeogenesis in the intact mouse liver, *Cell Metab. 5*, 313−320.
7. Valera, A., Pujol, A., Pelegrin, M., and Bosch, F. (1994) Transgenic mice overexpressing phosphoenolpyruvate carboxykinase develop non-insulin-dependent diabetes mellitus, *Proc. Natl. Acad. Sci. U.S.A. 91*, 9151−9154.
8. Gomez-Valades, A. G., Vidal-Alabro, A., Molas, M., Boada, J., Bermudez, J., Bartrons, R., and Perales, J. C. (2006) Overcoming diabetes-induced hyperglycemia through inhibition of hepatic phosphoenolpyruvate carboxykinase (GTP) with RNAi, *Mol. Ther. 13*, 401.
9. Croniger, C. M., Chakravarty, K., Olswang, Y., Cassuto, H., Reshef, L., and Hanson, R. W. (2002) Phosphoenolpyruvate carboxykinase revisited II. Control of PEPCK-C gene expression, *Biochem. Mol. Biol. Educ. 30*, 353−362.
10. Croniger, C. M., Olswang, Y., Reshef, L., Kalhan, S. C., Tilghman, S. M., and Hanson, R. W. (2002) Phosphoenolpyruvate carboxykinase revisited-Insights into its metabolic role, *Biochem. Mol. Biol. Educ. 30*, 14−20.
11. Hanson, R. W., and Patel, Y. M. (1994) Phosphoenolpyruvate carboxykinase (GTP): The gene and the enzyme, *Adv. Enzymol. Relat. Areas Mol. Biol. 69*, 203−281.
12. Hanson, R. W., and Reshef, L. (1997) Regulation of phosphoenolpyruvate carboxykinase (GTP) gene expression, *Annu. Rev. Biochem. 66*, 581−611.
13. Holyoak, T., Sullivan, S. M., and Nowak, T. (2006) Structural insights into the mechanism of PEPCK catalysis, *Biochemistry 45*, 8254−8263.
14. Delbaere, L. T. J., Sudom, A. M., Prasad, L., Leduc, Y., and Goldie, H. (2004) Structure/function studies of phosphoryl transfer by phosphoenolpyruvate carboxykinase, *Biochim. Biophys. Acta−Proteins Proteomics 1697*, 271−278.
15. Matte, A., Tari, L. W., Goldie, H., and Delbaere, L. T. (1997) Structure and mechanism of phosphoenolpyruvate carboxykinase, *J. Biol. Chem. 272*, 8105−8108.
16. Sudom, A. M., Prasad, L., Goldie, H., and Delbaere, L. T. J. (2001) The phosphoryl-transfer mechanism of *Escherichia coli* phosphoenolpyruvate carboxykinase from the use of AlF3, *J. Mol. Biol. 314*, 83−92.
17. Tari, L. W., Matte, A., Goldie, H., and Delbaere, L. T. J. (1997) Mg^{2+}-Mn^{2+} clusters in enzyme-catalyzed phosphoryl-transfer reactions, *Nat. Struct. Biol. 4*, 990−994.
18. Chen, C. Y., Sato, Y., and Schramm, V. L. (1991) Isotope trapping and positional isotope exchange with rat and chicken liver phosphoenolpyruvate carboxykinases, *Biochemistry 30*, 4143−4151.
19. Konopka, J. M., Lardy, H. A., and Frey, P. A. (1986) Stereochemical course of thiophosphoryl transfer catalyzed by cytosolic phosphoenolpyruvate carboxykinase, *Biochemistry 25*, 5571−5575.
20. Sheu, K. F., Ho, H. T., Nolan, L. D., Markovitz, P., Richard, J. P., Utter, M. F., and Frey, P. A. (1984) Stereochemical course of thiophosphoryl group transfer catalyzed by mitochondrial phosphoenolpyruvate carboxykinase, *Biochemistry 23*, 1779−1783.
21. Dunten, P., Belunis, C., Crowther, R., Hollfelder, K., Kammlott, U., Levin, W., Michel, H., Ramsey, G. B., Swain, A., Weber, D., and Wertheimer, S. J. (2002) Crystal structure of human cytosolic phosphoenolpyruvate carboxykinase reveals a new GTP-binding site, *J. Mol. Biol. 316*, 257−264.
22. Matte, A., Goldie, H., Sweet, R. M., and Delbaere, L. T. (1996) Crystal structure of *Escherichia coli* phosphoenolpyruvate carboxykinase: A new structural family with the P-loop nucleoside triphosphate hydrolase fold, *J. Mol. Biol. 256*, 126−143.
23. Matte, A., Tari, L. W., and Delbaere, L. T. (1998) How do kinases transfer phosphoryl groups? *Structure 6*, 413−419.
24. Miller, R. S., Mildvan, A. S., Chang, H. C., Easterday, R. L., Maruyama, H., and Lane, M. D. (1968) The enzymatic carboxylation of phosphoenolpyruvate. IV. The binding of manganese and substrates by phosphoenolpyruvate carboxykinase and phosphoenolypyruvate carboxylase, *J. Biol. Chem. 243*, 6030−6040.
25. Gasteiger, E., Hoohland, C., Gattiker, A., Duvaud, S., Wilkins, M. R., Appel, R. D., and Bairoch, A. (2005) Protein identification and analysis tools on the ExPASy server, in *The Proteomics Protocols Handbook* (Walker, J. M., Ed.) pp 571−607, Humana Press, Totowa, NJ.
26. Luft, J. R., Collins, R. J., Fehrman, N. A., Lauricella, A. M., Veatch, C. K., and DeTitta, G. T. (2003) A deliberate approach to screening for initial crystallization conditions of biological macromolecules, *J. Struct. Biol. 142*, 170−179.
27. Otwinowski, Z., and Minor, W. (1997) Processing of X-ray diffraction data collected in oscillation mode, in *Methods in Enzymology* (Carter, C. W., Jr., and Sweet, R. M., Eds.) pp 307−326, Academic Press, New York.
28. Vagin, A., and Teplyakov, A. (1997) MOLREP: An automated program for molecular replacement, *J. Appl. Crystallogr. 30*, 1022−1025.
29. Bailey, S. (1994) The Ccp4 Suite—Programs for protein crystallography, *Acta Crystallogr. Sect. D: Biol. Crystallogr. 50*, 760−763.
30. Emsley, P., and Cowtan, K. (2004) Coot: Model-building tools for molecular graphics, *Acta Crystallogr. D: Biol. Crystallogr. 60*, 2126−2132.
31. Colombo, G., Carlson, G. M., and Lardy, H. A. (1978) Phosphoenolpyruvate carboxykinase (guanosine triphosphate) from rat liver cytosol. Separation of homogeneous forms of the enzyme with high and low activity by chromatography on agarose-hexane-guanosine triphosphate, *Biochemistry 17*, 5321−5329.
32. Noce, P. S., and Utter, M. F. (1975) Decarboxylation of oxalacetate to pyruvate by purified avian liver phosphoenolpyruvate carboxykinase, *J. Biol. Chem. 250*, 9099−9105.
33. Painter, J., and Merritt, E. A. (2005) A molecular viewer for the analysis of TLS rigid-body motion in macromolecules, *Acta Crystallogr. Sect. D: Biol. Crystallogr. 61*, 465−471.
34. Laskowski, R. A., Macarthur, M. W., Moss, D. S., and Thornton, J. M. (1993) Procheck—A program to check the stereochemical quality of protein structures, *J. Appl. Crystallogr. 26*, 283−291.

35. Hlavaty, J. J., and Nowak, T. (1997) Affinity cleavage at the metal-binding site of phosphoenolpyruvate carboxykinase, *Biochemistry 36*, 15514−15525.
36. Hlavaty, J. J., and Nowak, T. (1997) Formation and characterization of an active phosphoenolpyruvate carboxykinase-cobalt(III) complex, *Biochemistry 36*, 3389−3403.
37. Tari, L. W., Matte, A., Pugazhenthi, U., Goldie, H., and Delbaere, L. T. (1996) Snapshot of an enzyme reaction intermediate in the structure of the ATP-Mg2+-oxalate ternary complex of *Escherichia coli* PEP carboxykinase, *Nat. Struct. Biol. 3*, 355−363.
38. Cotelesage, J. J. H., Prasad, L., Zeikus, J. G., Laivenieks, M., and Delbaere, L. T. J. (2005) Crystal structure of Anaerobiospirillum succiniciproducens PEP carboxykinase reveals an important active site loop, *Int. J. Biochem. Cell Biol. 37*, 1829.
39. Holyoak, T., and Nowak, T. (2004) pH Dependence of the reaction catalyzed by avian mitochondrial phosphoenolpyruvate carboxykinase, *Biochemistry 43*, 7054−7065.
40. Cheng, K. C., and Nowak, T. (1989) Arginine residues at the active site of avian liver phosphoenolpyruvate carboxykinase, *J. Biol. Chem. 264*, 3317−3324.
41. Jabalquinto, A. M., Laivenieks, M., Zeikus, J. G., and Cardemil, E. (1999) Characterization of the oxaloacetate decarboxylase and pyruvate kinase-like activities of *Saccharomyces cerevisiae* and *Anaerobiospirillum succiniciproducens* phosphoenolpyruvate carboxykinases, *J. Protein Chem. 18*, 659−664.
42. Jomain-Baum, M., and Schramm, V. L. (1978) Kinetic mechanism of phosphoenolpyruvate carboxykinase (GTP) from rat liver cytosol. Product inhibition, isotope exchange at equilibrium, and partial reactions, *J. Biol. Chem. 253*, 3648−3659.
43. Guidinger, P. F., and Nowak, T. (1991) An active-site lysine in avian liver phosphoenolpyruvate carboxykinase, *Biochemistry 30*, 8851−8861.
44. Krautwurst, H., Bazaes, S., Gonzalez, F. D., Jabalquinto, A. M., Frey, P. A., and Cardemil, E. (1998) The strongly conserved lysine 256 of *Saccharomyces cerevisiae* phosphoenolpyruvate carboxykinase is essential for phosphoryl transfer, *Biochemistry 37*, 6295−6302.
45. Brunger, A. T. (1992) Free R-value−A novel statistical quantity for assessing the accuracy of crystal structures, *Nature 355*, 472−475.
46. Potterton, E., McNicholas, S., Krissinel, E., Cowtan, K., and Noble, M. (2002) The CCP4 molecular-graphics project, *Acta Crystallogr. Sect. D: Biol. Crystallogr. 58*, 1955−1957.
47. Potterton, L., McNicholas, S., Krissinel, E., Gruber, J., Cowtan, K., Emsley, P., Murshudov, G. N., Cohen, S., Perrakis, A., and Noble, M. (2004) Developments in the CCP4 molecular-graphics project, *Acta Crystallogr. Sect. D: Biol. Crystallogr. 60*, 2288−2294.
48. Cotelesage, J. J. H., Puttick, J., Goldie, H., Rajabi, B., Novakovski, B., and Delbaere, L. T. J. (2007) How does an enzyme recognize CO_2? *Int. J. Biochem. Cell Biol. 39*, 1204−1210.

BI701038X